2-11 A Spectroscopic Study of Ion Channels in a Prototype Inertial Electrostatic Confinement Reactor

S. Collis and J. Khachan
School of Physics, Sydney University
NSW 2006, Australia

Inertial Electrostatic Confinement (IEC) involves using a semi-transparent and negatively biased grid to accelerate light nuclei towards a common centre for the purpose of generating neutrons through fusion reactions.

This project investigated the plasma properties in a small prototype IEC device that was operated using a relatively low grid bias in a discharge of hydrogen. Electrostatic lenses, which are the product of the geometry of the grid, create ion channels. Doppler shift spectroscopy was performed on the emission produced by charge exchange reactions in these channels.

Using the spectra we obtained, we were able to determine energies, ratios of hydrogen species (H^+:H_2^+:H_3^+) and thermal properties of ions present in these channels.

A discussion of results will be presented with particular emphasis on the implications of our findings to the construction of a portable neutron production device.

1.Introduction

Although Tokamaks have long been thought to be the best option as a fusion reactor, they lack the simplicity and portability that would be desired of a small-scale neutron production facility.

This report is about an investigation into an alternate method for initiating fusion reactions to produce neutrons: Inertial Electrostatic Confinement (IEC). The primary aim of this project was an investigation of fundamental plasma properties in an IEC device, with a particular focus on ion beams generated in such a device.

In the short term it is envisaged that IEC devices will be used as small portable sources of neutrons for applications such as elemental analysis of materials and medical treatments.

2.Grid Configurations

The three ring grid (figure 2.1a) was made by spot welding three stainless steel rings together. Stainless steel was chosen because it is non-magnetic. The outer grid (figure 2.1b) was constructed from a brass mesh which was welded onto a stainless steel supporting structure.

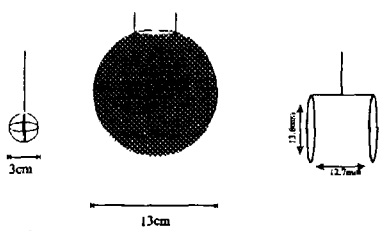

Figure 2.1
IEC grid configurations

Our experiments were focused on the ion channels. A three ring grid (figure 2.1a) can be thought of as eight closed loops which creates four opposing loop pairs. Ion channels were observed (figure 2.2) to form in the centres of these loops.

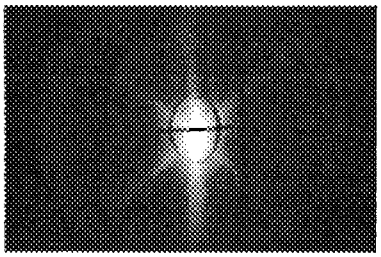

figure 2.2
Ion Channels in an IEC reactor

Many of the measurements were carried out on one channel since all channels were identical. To achieve this, we used a grid (figure 2.1c) which was made from two rings with a diameter of 13.6 mm. These are designed to form electrostatic lenses similar to those formed by two opposing triangles of the three ring grid.

3.Plasma Generation

Hirsch used an oxide coated outer grid as a source of electrons to generate a plasma when the inner grid potential was turned on, resulting in a DC discharge. In our experiment, we decided to look at an IEC system that has a separate plasma generating system. To maintain spherical symmetry, the plasma produced must be relatively uniform around the outer grid and the signal used to generate the plasma must not interfere with the plasma dynamics inside the outer grid.

Our system consists of a lower chamber (which was not used in our experiments), a glass tube (G) with a single loop antenna (H) and an upper processing chamber:

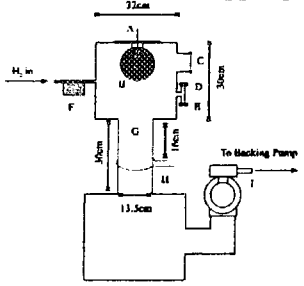

Figure 3.1
Experimental setup

A	High voltage feed through
B	IEC inner and outer grids
C	Quartz window
D	Capacitance Manometer
E	Ion gauge Manometer
F	Mass flow controller
G	Glass discharge tube
H	Single loop antenna connected to matching network
I	Turbo molecular pump

In its normal mode of operation, a 13.56 MHz radio frequency generator connected to the antenna (H) excites (primarily) the m = 0 mode of a helicon wave, but for our purposes the

antenna was used to inductively generate a plasma. When the rf generator (connected to the single loop antenna / matching network) is operated at 10W it produced a low density (~10^{10} cm^{-3}) low temperature plasma (T_e~1eV, T_i~0.03eV).

4.Potential Calculations

To find the potential between a biased inner grid and the earthed outer grid Poisson's equation must be solved. In a vacuum this reduces to Laplace's equation:

$$\nabla^2 V(x,y,z) = 0 \tag{4.1}$$

The geometry of the grids used in our experiments impose boundary conditions which lack the simplifying symmetries regularly used to solve equation (4.1). So instead, we assume that the potential is due to rings of charge (in the shape of the grid). If we have a distribution of point charges at x_n, y_n, z_n with charges q_n, the potential at an arbitrary point x, y, z is:

$$V(x,y,z) = \frac{1}{4\pi\varepsilon_0}\sum_n q_n\left((x_n - x)^2 + (y_n - y)^2 + (z_n - z)^2\right)^{-1/2} \tag{4.2}$$

After running the simulation, the validity of the model was checked by plotting an equi-potential surface (or iso-surface), using the visualisation and data processing package AVS, at the grid potential:

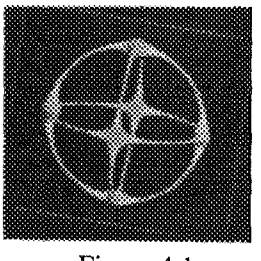

Figure 4.1
Equipotential surface at the grid potential

As shown in figure 4.1, the model produces a "virtual wire". This is a grid which is an exact solution to the model we used. The virtual grid closely resembles the real grid except for where the approximation breaks down at the wire joins. This is due to our charges having a fixed position which does not allow them to redistribute themselves to maintain a uniform charge density at a join (the charge density around any one given ring is uniform, but at a join the two rings come into contact and the density increases).

One plane of potentials that is of particular interest is that which contains the centres of the two triangles, that is, in the plane of an ion channel. Figure 4.3b shows contours (equi-potential lines) of the potential well. Each contour has a thickness of $0.2V/V_{grid}$, where V_{grid} is the potential of the grid. Figure 4.3a shows the plane in which the contours of figure 4.3b were taken:

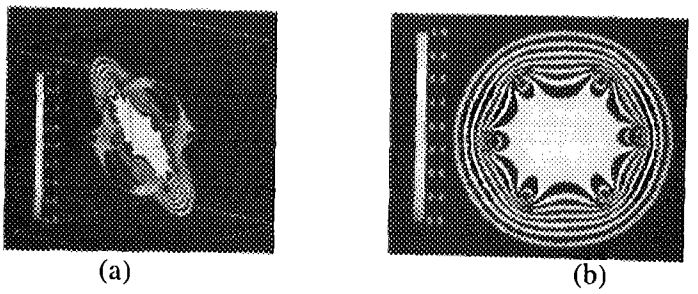

(a) (b)

Figure 4.3
Threshold contour plots of potential well structures

As previously stated, our approximation only breaksdown near the welding joints, so this plot is perfectly valid since it is far enough away from the joints.

5.Optical Setup

Light from the discharge exited the vacuum chamber through port (C) (in figure 3.1) where it was focused by a lens with a focal length of 15 centimetres.

For the spectra taken in this experiment we used an Optical Multi-channel Analyser (OMA). The OMA has two components: A 500mm monochromator with a 2400 lines per mm grating and a intensified CCD array detector (see figure 5.5).

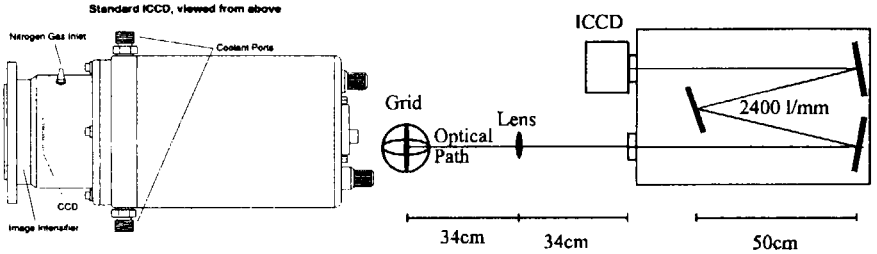

Figure 5.5
Optical setup

To further reduce thermal noise, the entire intensifier-CCD assembly was cooled to -30°C by a Peltier cooler and dry nitrogen flowed over the array to stop water vapour freezing onto the chip and causing it to crack.

6. Charge Exchange

The following charge exchange reactions between hydrogen ions and atomic hydrogen can occur[1], where the underlined species have approximately the same velocity:

$$\begin{aligned} \underline{H^+} + H &\longrightarrow \underline{H^*} + H^+ \\ \underline{H_2^+} + H &\longrightarrow \underline{H^*} + \underline{H} + H^+ \\ \underline{H_3^+} + H &\longrightarrow \underline{H^*} + \underline{H_2} + H^+ \end{aligned} \qquad (6.1)$$

where the superscript * refers to an excited state.

If the neutral species is molecular hydrogen, the following reactions occur:

$$\begin{aligned} \underline{H^+} + H_2 &\longrightarrow \underline{H^*} + H_2^+ \\ \underline{H_2^+} + H_2 &\longrightarrow \underline{H^*} + \underline{H} + H_2^+ \\ \underline{H_3^+} + H_2 &\longrightarrow \underline{H^*} + \underline{H_2} + H_2^+ \end{aligned} \qquad (6.2)$$

Because the atom is initially neutral, the sum of the energies of the resulting neutrals is close to the energy of the ion that caused the event. McClure[2] experimentally determined the charge exchange differential cross-section for a variety of incident ion energies. The differential cross-section for charge exchange reactions between H_2 molecules and 10keV H^+ ions is shown in figure 6.1 below.

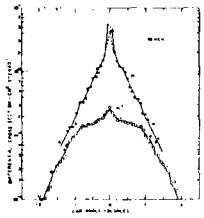

Figure 6.1
Differential cross-section for a charge exchange reaction between H^+ and H_2^+ at 10keV

Figure 6.1 shows that the number of particles that will be scattered into angles greater than 2 degrees is very small. From this we can conclude that charge exchange products do not deviate significantly from the path of the incoming ion.

7.Two Ring Spectral Profile

Below is a spectrum taken from the two ring grid. The spectrum is a line of emission integral. The intensity is greatest in the centre of the grid, which contains very weak (negligible) electric fields.

There are a few important facts to note: The emitters (from the reactions in equation 6.2) are all neutral hydrogen atoms so there are no metastable states or molecular transitions. Also, according to Volger[3] the resulting hydrogen fragments (in equation 6.2) resulting from an H_2^+ or H_3^+ impact event have approximately the same velocity (The difference in energy is approximately 0.5eV).

The spectrum below (figure 7.1a) contains a total of ten peaks. This was not completely obvious until a detailed analysis of the system was done.

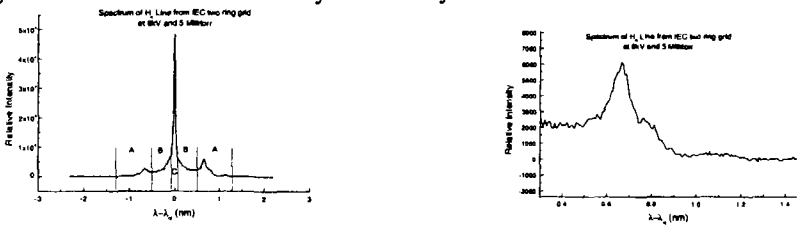

(a) (b)

Figure 7.1
Components of the Hα spectrum

Region A (in figure 7.1a, also enlarged in figure 7.1b) is due to the incoming and outgoing ion beams. This region contains six (three incoming and three outgoing) beams due to three different species of hydrogen ions.

Region B is due to a thermal background. It is the emission due to three Maxwellian velocity distributions for the three different masses of the ions. It is envisaged that this background is formed by ion scattering due to columbic collisions with the other oncoming beam and possibly becoming thermalised.

Region C (in figure 7.1a) is due to dissociative excitation of the neutral hydrogen, which is stationary in the lab frame. Charged species gain energy from the electric field produced by the grid. Energy is transferred between ions through columbic collisions. However, the cross section for collisions between neutral and ionic hydrogen is much smaller than the coulomb collision cross-section. As a result, the temperature of the gas was near room temperature (~300 K). This will yield a half width of 0.005 Angstroms. Since this value is sufficiently small we used the width of this line to determine the instrumental broadening.

8.Three Ring Profile

The spectra presented in this section was recorded by Kristie Foulkes[4]. Spectra were recorded for voltages ranging from 1 kV (B) to 12 kV (M). The pressure was kept at ~5 millitorr.

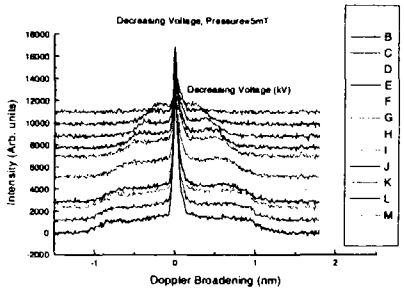

Figure 8.1
Varation of the H_α line with grid potential
Adopted from [4]

Spectra shown in figure 8.1 contain the same features as the spectra for the two ring grid but have four peaks due to charge exchange (one for each ion beam). From the wavelength at which our signal drops below the noise level we found that the maximum energy that an ion reaches was 27% of the vacuum well depth.

9.Quantities Obtained from the Two Ring Grid Spectra

By fitting Gaussians to each of the peaks present in the three ring grid we were able to observe changes in beam energy, ion temperate and relative density (by doing rate equation modeling), with respect to the grid potential.

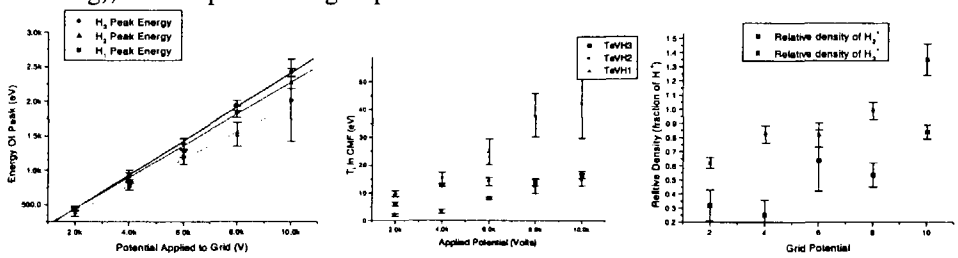

Figure 9.1
Variation of plasma properties with grid potential

The energies of the three species are equal, however due to their different mobilities the are collisionally heated (due to collisions with the background gas) differentially.

10.Conclusion

We have shown that when a three ring grid is immersed in a plasma ion channels are formed due to electrostatic lenses formed by the grid wires. The ion beams formed consist of H^+, H_2^+ and H_3^+ and have an energy equal to 27% of the vacuum electrostatic potential well depth. We have also shown that, due to increased collisions with background gasses, the beams are heated when the potential is increased (which results in an increased beam flux).

References

[1] C Barbeau J Jolly *J. Phys. D: Appl. Phys.* **23**, 1168 (1990)
[2] G McClure *Phys. Rev 3A* **140**, 769 (1965)
[3] M Volger, *Z. Physik A* **7-10**, 288 (1978)
[4] Kristie Foulkes, Physics III project